



Article

Preparation and Characterization of Fe-Mn Binary Oxide/Mulberry Stem Biochar Composite Adsorbent and Adsorption of Cr(VI) from Aqueous Solution

Meina Liang^{1,2}, Shuiping Xu¹, Yinian Zhu^{1,2,*}, Xu Chen¹, Zhenliang Deng¹, Liling Yan¹ and Huijun He^{1,2}

¹ College of Environmental Science and Engineering, Guilin University of Technology, Guilin 541004, China; liangmeinaa@163.com (M.L.); shuipingxuu@163.com (S.X.); benrenchenxu@163.com (X.C.); dengzhenliang088@163.com (Z.D.); yanlilingg@163.com (L.Y.); hehj@glut.edu.cn (H.H.)

² Guangxi Key Laboratory of Environmental Pollution Control Theory and Technology, Guilin 541004, China

* Correspondence: zhuyinian@glut.edu.cn; Tel.: +86-130-7769-2937

Received: 20 December 2019; Accepted: 17 January 2020; Published: 21 January 2020



Abstract: This study details the preparation of Fe-Mn binary oxide/mulberry stem biochar composite adsorbent (FM-MBC) from mulberry stems via the multiple activation by potassium permanganate, ferrous chloride, triethylenetetramine, and epichlorohydrin. The characteristics of FM-MBC had been characterized by SEM-EDS, BET, FT-IR, XRD, and XPS, and static adsorption batch experiments such as pH, adsorption time, were carried out to study the mechanism of Cr(VI) adsorption on FM-MBC and the impact factors. The results indicated that in contrast with the mulberry stem biochar (MBC), the FM-MBC has more porous on surface with a BET surface area of 74.73 m²/g, and the surface loaded with α -Fe₂O₃ and amorphization of MnO₂ particles. Besides, carboxylic acid, hydroxyl, and carbonyls functional groups were also formed on the FM-MBC surface. At the optimal pH 2.0, the maximum adsorption capacity for Cr(VI) was calculated from the Langmuir model of 28.31, 31.02, and 37.14 mg/g at 25, 35, and 45 °C, respectively. The aromatic groups, carboxyls, and the hydroxyl groups were the mainly functional groups in the adsorption of Cr(VI). The mechanism of the adsorption process of FM-MBC for Cr(VI) mainly involves electrostatic interaction, surface adsorption of Cr(VI) on FM-MBC, and ion exchange.

Keywords: mulberry stem; bio-charcoal; adsorption; Fe-Mn binary oxide; chromium

1. Introduction

With the rapid development of industrialization, chromium-containing compounds has been extensively used in industrial production, such as tanning, electroplating, dyeing, and coloring pigments [1,2]. China is one of the primary chromium producing countries. There are about 25 firms manufacturing chromium salts, and the chromium salts of these firms could reach 329,000 tons every year [3]. Chromium principally exists in Cr(III) and Cr(VI) oxidation states [4,5]. The toxicity of Cr(VI) is five hundred times that of Cr(III). Cr(VI) may cause teratogenesis, mutation, or carcinogenesis for living creatures [6] and has been chosen as a priority pollutant by the USEPA [7]. The maximum concentrations of Cr(VI) set by the Environmental Protection Agency in industrial wastewater and drinking water were 200 and 50 µg/L, respectively [8].

Currently, the main techniques for removing chromium include ion exchange, membrane separation, electrolytic removal, chemical reduction, and adsorption [8]. Among these methods, as one of the most promising techniques, adsorption technology has been employed for a several decade years, and the effectiveness has been demonstrated [9]. Biochar has less porosity and more surface oxygen-containing functional groups than activated carbon [10]. These characteristics show that

biochar has a strong ion exchange capacity and has been used to adsorb organic contaminants, heavy metals, and other pollutants and for environmental remediation, etc. [11–13]. Guangxi province is located in the southeast China. The annual output of mulberry stem in Guangxi is about 1 million tons, which are frequently burned due to share utilization technology of mulberry stem [14]. Once mulberry stem was burned in the fields, which not only caused air pollution but also caused resource waste. Mulberry is rich in cellulose and hemicellulose, it can be used as an important feedstock for biochar production because mulberry stem is an adequate, renewable, and low-cost biomass.

Because of the high adsorption affinity and special surface activity, manganese and iron oxide powders have been extensively studied and have been widely used to remove heavy metals [15]. MnOx are also significant scavengers to various ions in contaminated water [16]. Iron oxide has been used in most studies for the modification of biochar or other materials, since it has a natural affinity to chromium [17]. Besides, ferrimanganic binary oxide adsorbents have been widely targeted for removing heavy metals from water due to their valid performance, environmentally friendly properties, and low cost [18]. Wang et al. [19] discovered that FMBC (Biochar impregnated with iron and manganese oxides) indicated improved sorption of Cr(VI) compared with biochar. Iron manganese bimetal oxide nanospheres were synthesized via a facile and environmentally friendly template-free approach, and the maximum adsorption capacities of Cr(VI) was 105.96 mg/g [20]. Du et al. [21] prepared a granular Fe-Mn binary oxide and used it to remove Cr(VI) from aqueous solution, and the maximum adsorption abilities for Cr(VI) was higher than other granular adsorbents for Cr(VI) adsorption. Moreover, Fe-Mn binary oxide adsorbents can increase the pH_{zpc} values of biochar and strongly dominate the charge properties. These are beneficial for the adsorption of chromium in the anionic state [22]. Given all the analysis above, the Ferro-manganese binary oxide with biochar can combine the advantages of manganese and iron oxides, showing strong adsorption capacity for heavy metal.

The purpose of this study is to assess the adsorption capacity of FM-MBC and MBC to Cr(VI), addressing the following specific objectives: (i) preparation and characterization of FM-MBC and MBC and (ii) investigation of the adsorption properties and adsorption mechanism of Cr(VI) by FM-MBC.

2. Experimental Part

2.1. Chemical Reagents and Solutions

Reagents purchased from Shanghai Guoyao Group Chemical Reagent Co. Ltd., China, including $FeCl_2 \cdot 4H_2O$, $MgCl_2 \cdot 6H_2O$, $KMnO_4$, $K_2Cr_2O_7$, HNO_3 , NaOH, Polyethylene glycol (PEG), triethylenetetramine, etc., were analytical reagent grade. The standard solution of Cr(VI) (1000 mg/L) was purchased from National Nonferrous Metals and Electronic Materials Analysis and Testing Center, China, stored at 4 °C. Conductivity of the experimental water greater than 18.2 MΩ cm (Millipore-Q Direct 8) was used throughout.

2.2. Preparation of FM-MBC

The preparation of Mulberry stem biochar (MBC) and FM-MBC was based on the method reported by Liang et al. (China Patent No. 201811047535.9). The peeled mulberry was smashed about a particle size of 1 mm and then was dried in oven at 80 °C for 24 h. The dry mulberry was carbonized/activated in a muffle furnace at 500 °C for 3 h to get the MBC, and then, it was sieved to a particle size of about 0.15 mm.

A total of 3 g of MBC was added into a 500 mL conical flask; then, 50 mL 0.2 mol/L $FeCl_2$ aqueous solution and 0.05 M $MgCl_2$ aqueous solution were added into the conical flask rapidly under magnetic stirring for 10 min, and the conical flask was covered with a glass surface dish to impregnate for 3 h. Then 1 mL PEG, 100 mL 0.05 M $KMnO_4$ solution, 20 mL 2.5 M NaOH solution and 10 mL epichlorohydrin were added to the mixture suspended solution under magnetic stirring in turn. Under magnetic stirring, the mixture suspended solution continued to react for 3 h at 60 °C. Then 5 mL triethylenetetramine was added to the mixture suspended solution and continued to react for 6 h at

80 °C. After reaction, the suspended solid was cooled, then was filtered, and dried in oven at 65 °C to get the FM-MBC. Finally the FM-MBC was sifted by a 100 mesh sieve.

2.3. Characterization

The structural feature of MBC and the FM-MBC was observed using scanning electron microscopy (SEM, JSM-7900F, Joint-stock Company, Tokyo, Japan). Powder X-ray diffractometer equipped was used for the XRD analysis (X'Pert PROX, PANalytical, B.V., EA Almelo, Netherlands). Infrared spectra were measured using a PE CAT500A FTIR spectrometer (PerkinElmer, Liantrisant, UK). X-ray photoelectron spectroscopy (XPS) experiments of FM-MBC were performed by ESCALAB•250Xi (Thermo Electron Corporation, Massachusetts, USA). The zeta potential of materials was undertaken using a Nano-ZS90 apparatus (Malvern Panalytical, Worcestershire, UK) [23]. The specific surface area of MBC and FM-MBC were determined according to the BET equation by nitrogen gas adsorption using a JW-BK200C apparatus (Beijing Jingwei Gaobo science and Technology Co., Ltd. No.12 Kechuang 13th Street, Beijing Economic and Technological Development Zone, Beijing, China). The content of C, H, N, and S of samples was determined by Perkin Elmer Series IICHNS/O Analyzer 2400 (PerkinElmer, Shelton, USA).

2.4. Batch Experiment

The adsorption procedure was as follows, 0.100 g FM-MBC was added in 100 mL polyethylene plastic centrifuge tube; then, 50.0 mL Cr(VI) containing solution was added. The pH value of the solutions was adjusted by 0.1 M sodium hydroxide solution and/or nitric acid solution. The tubes were shaken at desired temperature and time at 200 rpm in a water bath oscillator. Then the mixture was separated by centrifugation, and supernatant was carefully filtered; then, the concentration of Cr(VI) was measured using diphenylcarbazide spectrophotometry.

The Effect of pH was studied from 2.0 to 11.0 (pH 2.0, 3.0, 4.0, 5.0, 6.0, 7.0, 8.0, 9.0, 10.0, 11.0) and the Cr(VI) containing solutions (10 or 20 mg/L) mixed with FM-MBC and shaken for 24 h at 25 °C. To obtain the adsorption isotherms, solutions of various Cr(VI) concentrations (2, 5, 10, 20, 30, 40, 50, 60, 80, 100, 120, 150 mg/L) were shaken with the FM-MBC for 24 h. The effect of the contact time of Cr(VI) adsorption onto FM-MBC was carried out in 50 mL of 10 and 20 mg/L Cr(VI) solution, and the concentration of Cr(VI) was analyzed at different time (0.25, 0.5, 1, 2, 3, 4, 5, 6, 8, 10, 12, 15, 18, 21, 24, 27, 30, 36, 48 h).

3. Results and Discussion

3.1. Characterization of FM-MBC

3.1.1. Elemental Analysis and Specific Surface Area

Elemental analysis results (Table S1) indicated that accounting carbon elements were 77.4% and 57.29% in the MBC and FM-MBC, respectively. Oxygen element accounting in MBC increased from 8.94% to 28.31% in FM-MBC; maybe some surface oxygen functional groups were formed on the FM-MBC surface [18]. The specific surface area of FM-MBC was 74.73 m²/g by the nitrogen adsorption–desorption method (BET-N₂). The pore volume of FM-MBC was 0.094 cm³/g.

3.1.2. SEM Analysis

The SEM of MBC and FM-MBC was shown in Figure 1; it was found that the MBC had smooth round shape and pore structure. The pore diameter of FM-MBC was between 0.5 and 5.0 μm, which was smaller than the pore diameter of MBC. The FM-MBC possessed more porous on the surface in contrast with the MBC and was loaded with iron and/or manganese oxide particles. Moreover, no collapse or failure on the wall surface of pore of FM-MBC was found. However, the surface of the FM-MBC became rough, and micropores with a pore diameter of less than 1 μm were increased. The micropore

was beneficial to the internal diffusion of adsorbents for heavy metal ions [24]. Numerous spherical dots were added to the inner wall of the pore and attached to the pore surface. These spherical dots may be metal oxides, which can provide more adsorption binding sites.

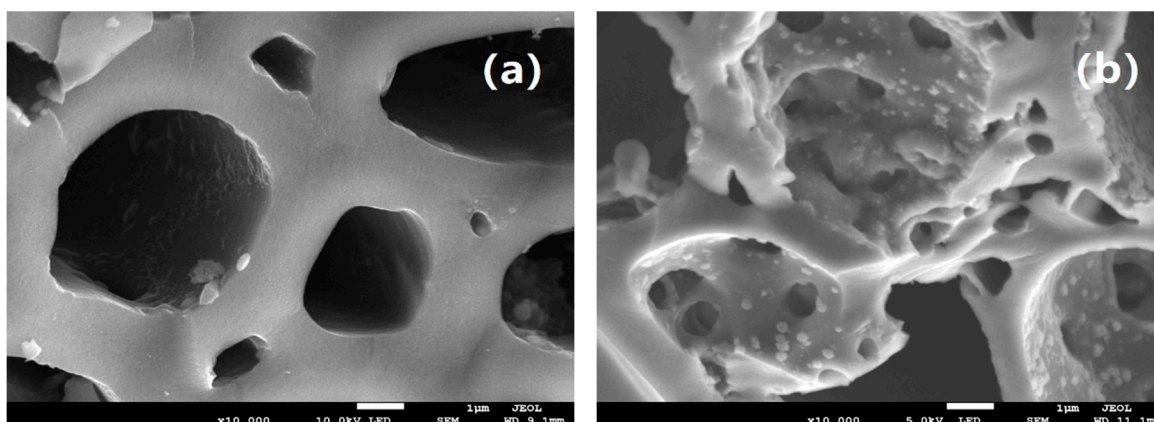


Figure 1. SEM image of mulberry stem biochar (MBC) and Fe-Mn binary oxide/mulberry stem biochar composite adsorbent (FM-MBC). (a) MBC, (b) FM-MBC.

3.1.3. XRD Analysis

The XRD patterns of the MBC and FM-MBC were shown in Figure 2. MBC exhibited one broad and gentle amorphous diffraction peak around at $2\theta = 24.2^\circ$; this was mainly the diffraction peak of crystalline carbon fibers. A strong diffraction peak was recorded at $2\theta = 29.5^\circ$ and exhibited some weak diffraction peaks at 36.1° , 39.4° , 43.3° , 47.6° , and 49.5° of 2θ value, which may be that the MBC was not cleaned and contained Ca, K, and Mg (Table S2). When MBC was loaded by Fe-Mn binary oxide, some weak diffraction peaks at 36.1° , 39.4° , 43.3° , 47.6° , and 49.5° of 2θ value disappeared, but a new weak diffraction peak at 35.5° was found. The new peak corresponded to $\alpha\text{-Fe}_2\text{O}_3$ standard peak (110) (PDF NO: 00-033-0664). Compared with MBC, no intensity crystalline typical peaks of MnO_2 were found of FM-MBC, which represented the formation of the amorphous phase of the FM-MBC [25,26].

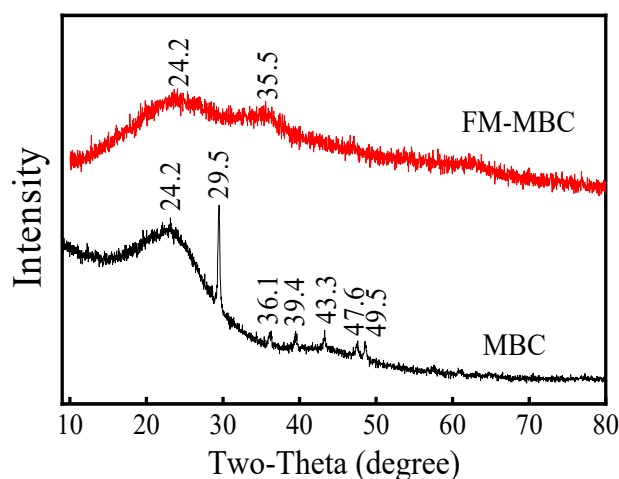


Figure 2. XRD spectrum of MBC and FM-MBC.

3.2. Effect of Solution pH

The pH value of the solution is a key factor affecting the removal of Cr(VI) [27], and the surface charge and dissociation of functional groups of biochar [28]. The amount adsorption of Cr(VI) gradually decreased as the pH value increased from 2.0 to 11.0. The optimal pH for Cr(VI) adsorption was 2.0, indicating that an acidic condition is favorable for the removal of Cr(VI). As shown in Figure S1,

the pH_{zpc} (point of zero charge) of FM-MBC was 7.4, so when the $pH < pH_{zpc}$, the surface of FM-MBC was positively charged, which was favorable for Chromium-containing anions were adsorbed on FM-MBC. Chromium-containing anions were mainly presented as $HCrO_4^-$ and $Cr_2O_7^{2-}$ in solution at pH range from 2.0 to 6.4 and as CrO_4^{2-} at $pH > 6.4$ [29]. Cr(VI) anions were adsorbed onto the positively charged FM-MBC surface by electrostatic interaction. When $pH > pH_{zpc}$, the surface of FM-MBC is negatively charged and caused electrostatic repulsion between the surface of FM-MBC and Chromium-containing anions, which has an adverse effect on Cr(VI) adsorption. At the same time, the OH^- occupying a part of the surface active adsorption site of the composite adsorbent to some degree, resulting in competitive adsorption of Cr(VI). This process reduced the removal effect of Cr(VI) by the adsorbent [30].

3.3. Effect of Adsorption Time

The effect of time on the adsorption of Cr(VI) on FM-MBC was shown in the Figure 3b. In terms of q_e -t relationship, the adsorption amount of Cr(VI) increased rapidly at the beginning of the adsorption experiment, indicating favorable interactions between FM-MBC and Cr(VI). The results in Figure 3b also showed that when the initial Cr(VI) concentration is 20 and 50 mg/L, the Cr(VI) adsorption amounts reached equilibrium at 2 and 3 h, respectively, at 25 °C and pH 2.0. It may be due to the fact that when Cr(VI) adsorption capacity was low in the initial reaction stage, the surface of the adsorbent contained numerous adsorption sites, and the adsorption reaction occurred rapidly [31]. The existence of lots of vacancies in the initial stage may be the reason for the rapid initial adsorption [32].

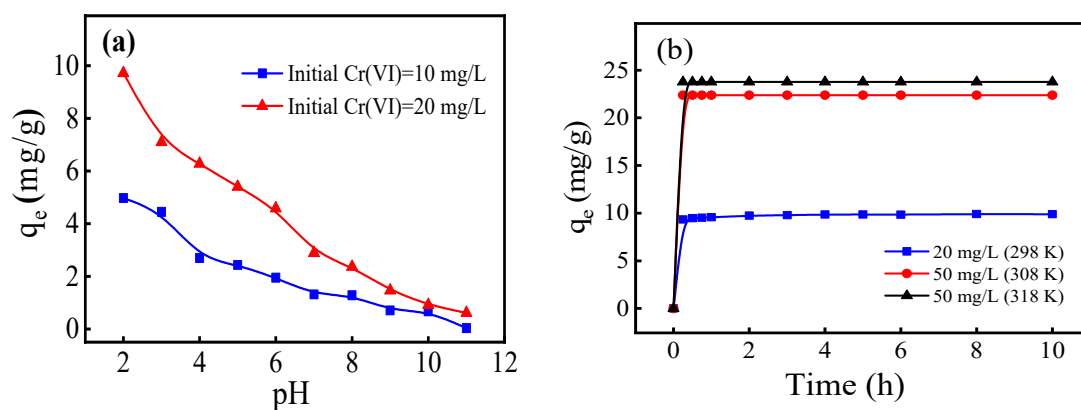


Figure 3. The effect of pH and contact time on Cr(VI) adsorption onto FM-MBC. (a) pH, (b) contact time.

3.4. Adsorption Kinetics

In this study, the Pseudo-first-order kinetic equation, Pseudo-second-order kinetic equation, Banghamkinetic equation, and Elovich kinetic equation were adopted to describe the adsorption kinetic data:

Pseudo-first-order Equation:

$$\ln(q_e - q_t) = \ln q_e - K_1 t \quad (1)$$

Pseudo-second-order Equation:

$$\frac{t}{q_t} = \frac{1}{k_2 q_e^2} + \frac{t}{q_e} \quad (2)$$

Bangham kinetic Equation:

$$\lg q_t = \lg k_3 + \frac{1}{m} \lg t \quad (3)$$

Elovich kinetic Equation:

$$q_t = a + k_4 \ln t \quad (4)$$

where q_e and q_t are the adsorption capacities of the adsorbent at equilibrium and at time t (min), respectively; k_1 (min^{-1}), k_2 ($\text{g}/\text{mg}\cdot\text{min}$), k_3 and k_4 are the Pseudo first-order kinetic constant, the Pseudo-second-order kinetic constant, the Bangham kinetic constant, the Elovich kinetic constant, respectively.

The fitting plots are shown in Figure 4 and the kinetic parameters acquired from fitting results are summarized in Table 1. The higher correlation coefficient (R^2) for the Pseudo-second-order equation implied that the adsorption processes of FM-MBC were controlled by chemisorption on their surface [33]. In addition, when the initial concentrations were 20 mg/L and 50 mg/L, the theoretical equilibrium adsorption amounts of Cr(VI) were 9.68 mg/g and 24.27 mg/g at 25 °C, respectively, which was very close to the actual measured equilibrium adsorption amounts (9.72 mg/g and 24.39 mg/g), indicating that these kinetic data conformed to the pseudo-second-order equation very well.

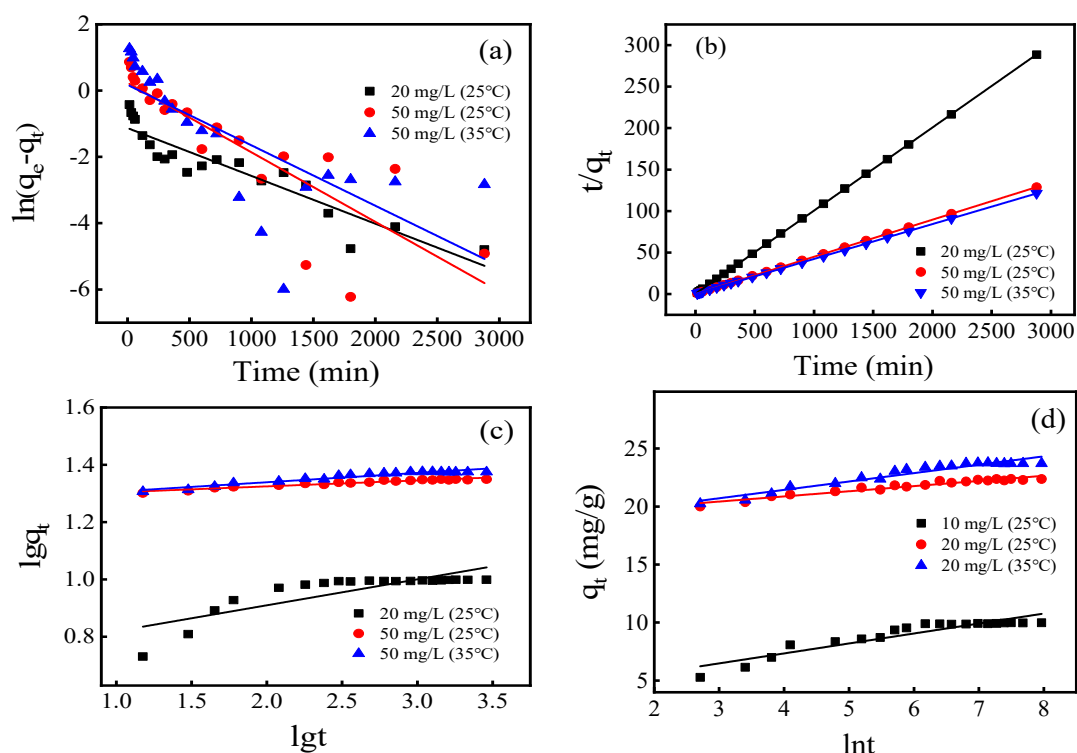


Figure 4. Adsorption kinetics of Cr(VI) adsorption on FM-MBC. (a) Pseudo-first-order, (b) Pseudo-second-order, (c) Banghamkinetic, (d) Elovich kinetic.

Table 1. Kinetic parameters for Cr(VI) adsorption onto the FM-MBC.

Concentration (mg/L)	q_e (mg/g)	Pseudo-First-Order Equation			Pseudo-Second-Order Kinetic Equation		
		R^2	k_1	q_m	R^2	k_2	q_m
20 (298 K)	9.72	0.858	0.0010	8.71	0.999	0.1002	9.68
50 (298 K)	24.39	0.786	0.0020	23.02	0.999	0.0447	24.27
50 (308 K)	24.57	0.913	0.0023	23.22	0.999	0.0420	24.43
Concentration (mg/L)	Bangham Kinetic Equation		Elovich Kinetic Equation				
	R^2	k_3	R^2	k_4			
20 (298 K)	0.674	0.091	0.869	0.858			
50 (298 K)	0.938	0.021	0.943	0.444			
50 (308 K)	0.923	0.032	0.925	0.723			

Kinetic Parameters

In the initial Cr(VI), concentration was 50 mg/L, and the influence of temperature on the FM-MBC adsorption Cr(VI) was investigated at 298 and 318 K. The Arrhenius equation was used to calculate activation energy (E_a) of adsorption as follows [34]:

$$\ln K_d = \ln A - \frac{E_a}{RT} \quad (5)$$

$$E_a = 2.303R \left(\frac{T_1 T_2}{T_1 - T_2} \right) \ln \frac{K_1}{K_2} \quad (6)$$

where A (g/mol·min), E_a (kJ/mol), R(8.3145 J/mol·K), T (K), K_d (g/mg·min), are the independent temperature factor, the activation energy of adsorption, the gas law constant, the solution absolute temperature and reaction rate constant of the pseudo-second-order equation, respectively. The activation energy is indicator for adsorption type, which for a physical adsorption E_a value lower than 40 kJ/mol and a chemisorption adsorption is higher than 40 kJ/mol. E_a was found to be 4.756 kJ/mol (E_a was calculated by Equation (6) with k_2 in Table 1 at 298 and 318 K). Base on the correlation coefficient (R^2) for the Pseudo-second-order and E_a value, it indicated that the FM-MBC adsorption Cr(VI) was a physical-chemical adsorption process [35].

3.5. Adsorption Isotherm

The adsorption isotherm of the MBC and FM-MBC for Cr(VI) (Figure 5), which indicated that the adsorption capacity of Cr(VI) rapidly increased, with increase in temperature at the equilibrium Cr(VI) concentration less than 10 mg/L. When the equilibrium concentration of Cr(VI) was greater than 10 mg/L, the adsorption capacity of Cr(VI) slowly increased. It may be due to the adsorbent not attaining adsorption saturation when the equilibrium concentration was lower and the adsorption reaction occurring on the surface of the adsorbent. The amount of Cr(VI) adsorbed increased from 0.20 to 28.31, 9.78 to 31.02, and 9.83 to 37.54 mg/g when the $C_{e(\text{Cr(VI)})}$ was increased from 0.01 to 43.52 mg/L, at 25, 35, and 45 °C, respectively. As the temperature increased from 25 to 45 °C, the amount of Cr(VI) adsorbed increased from 28.31 to 37.54 mg/g, indicating that increasing temperature was beneficial to Cr(VI) removal, and FM-MBC exhibited a Cr(VI) adsorption capacity higher about one point five times than that of MBC.

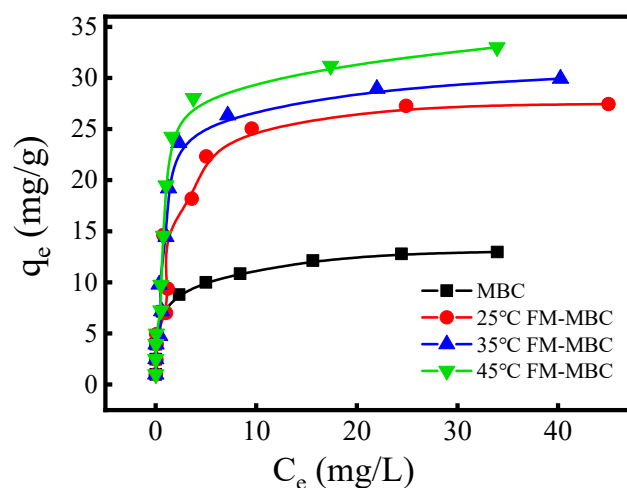


Figure 5. Adsorption isotherms of Cr(VI) adsorption on FM-MBC and MBC.

In this study, the Langmuir models and Freundlich models were applied to simulate the the experimental equilibrium data of the adsorption of Cr(VI) on the FM-MBC at of 25, 35, and 45 °C.

Langmuir Isotherm

Langmuir model can be represented by the equation as follows:

$$\frac{C_e}{q_e} = \frac{1}{(Q_{\max} \cdot K_L)} + \frac{C_e}{Q_{\max}} \quad (7)$$

where C_e means the Cr(VI) concentration of solution (mg/L) at adsorption equilibrium. The Q_{\max} represents the adsorption amount (mg/g), and K_L is the Langmuir constant (L/mg). The linear graph of plot of C_e/q_e versus C_e is shown in Figure 6. The values of Q_{\max} and K_L are calculated based on the slope and intercept of the linear graph (Table 2).

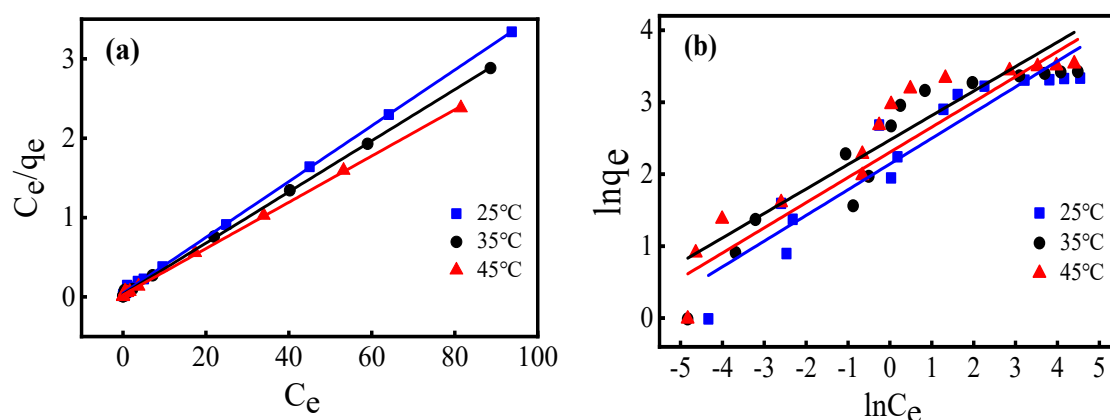


Figure 6. Isotherm plots for Cr(VI) adsorption onto FM-MBC. (a) Langmuir equation, (b) Freundlich equation.

Table 2. Isotherm parameters for Cr(VI) adsorption onto the FM-MBC.

Temperature °C	Langmuir Equation			Freundlich Equation		
	R ²	K _L	Q _{max} (mg/g)	R ²	K _F	1/n
25 (298 K)	0.999	1.107	28.49	0.875	17.274	0.357
35 (308 K)	0.999	1.215	31.21	0.866	19.038	0.350
45 (318 K)	0.999	1.224	37.62	0.871	22.301	0.341

The results of the fitting process in Figure 6 and Table 2 showed that Langmuir isotherm model is suitable for fitting the adsorption of chromium (VI) on FM-MBC. At 25, 35, and 45 °C, the correlation coefficients (R²) of Langmuir isotherm model are all 0.999. The results showed that homogeneous adsorption existed on the FM-MBC surface. The maximum adsorption capacity can be increased from 28.49 mg/g at 25 °C to 37.62 mg/g at 45 °C by increasing the temperature. The results showed that Cr(VI) adsorption on FM-MBC is endothermic. The adsorption capacity of FM-MBC for Cr(VI) at 25 °C is 28.49 mg/g, which is higher than 7.08 mg/g of municipal sludge biochar and 8.05 mg/g of yeast biochar [36,37], slightly higher than 21.45 mg/g of eucalyptus corm biochar [38].

Freundlich Isotherm

Freundlich model can be represented by the equation as follows:

$$\ln q_e = \ln K_F + \left(\frac{1}{n}\right) \ln C_e \quad (8)$$

In the formula, q_e is the adsorption capacity of Cr(VI) in equilibrium (mg/g), C_e is the equilibrium Cr(VI) concentration (mg/L), K_F (mg/g)/(mg/L)ⁿ is Freundlich constant, and 1/n is adsorption strength.

The K_F and 1/n values can be calculated from the plot of $\ln q_e$ versus $\ln C_e$ (Figure 7, Table 2). At 25, 35, and 45 °C, the correlation coefficients (R²) of the Freundlich isotherm model were 0.875, 0.866,

and 0.871, respectively, and the Freundlich isotherm could not well fit Cr(VI) adsorption on FM-MBC. $1/n$ can be used for measuring the deviation from linear of the adsorption [39,40]. In this study, $1/n$ values were 0.357 (25 °C), 0.350 (35 °C) and 0.341 (45 °C), which indicated that Cr(VI) adsorption onto FM-MBC process belong to be chemical adsorption [39].

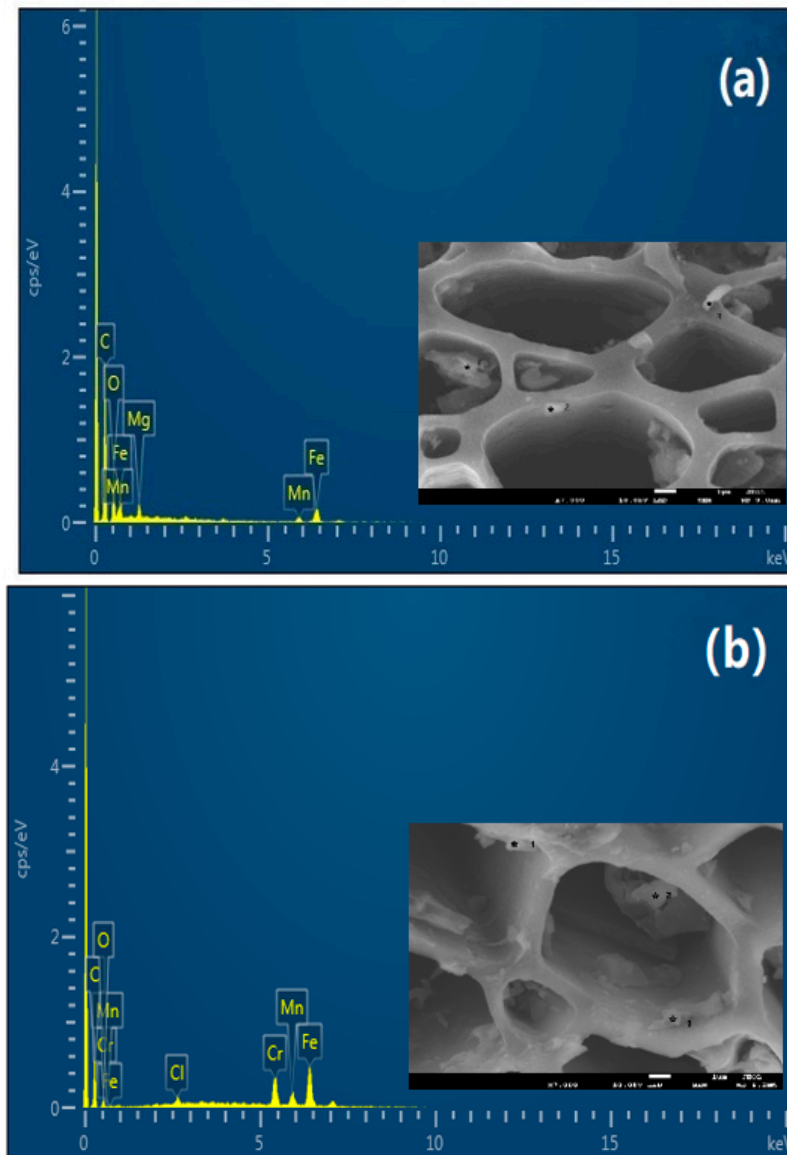


Figure 7. SEM-EDS spectrum of the FM-MBC. (a) FM-MBC, (b) FM-MBC after Cr(VI) adsorption.

Thermodynamic Parameters

Thermodynamic parameters can be calculated using Equations (9) and (10) [41].

$$\Delta G^\circ = -RT \ln K_L \quad (9)$$

$$\Delta G^\circ = -RT \ln K_L = \Delta H^\circ - T \Delta S^\circ \quad (10)$$

where ΔG° is changes in standard free energy; ΔH° is changes in standard enthalpy; ΔS° is changes in standard entropy; R , K_L , and T are gas constant, the Langmuir constant and the temperature in Kelvin (K), respectively.

ΔG° can be calculated by Equation (9). ΔH° and ΔS° can be calculated from the plot of ΔG° versus T. As shown in Table 2, the adsorption capacity of Cr(VI) increased with the temperature range from 25 to 45 °C, which indicated endothermic reaction occurred. ΔG° calculated by Equation (9) were -0.252 , -0.499 , and -0.528 kJ/mol at 25, 35, and 45 °C, respectively, which indicated that the adsorption for Cr(VI) on FM-MBC was spontaneous nature. At the same time, the positive ΔH° values (3.946 kJ/mol) suggested endothermic reaction occurred. Besides, the positive ΔS° values (0.1045 kJ/(mol K)) indicated that the randomness increased at the interface of the solid/solution during the adsorption of Cr (VI) on the FM-MBC [42].

3.6. Mechanism of Cr(VI) Adsorption by FM-MBC

3.6.1. SEM-EDS Analysis

The EDS analysis indicated that Mn, Fe, and O were presented in the FM-MBC powder before and after Cr(VI) adsorption, and Cr was presented in the FM-MBC powder after Cr(VI) adsorption (Figure 7). The mass percentages of elements were undertaken at three points (Table 3). According to the results of EDS spectrum, the means of mass percentages (%) of C, O, Mn, and Fe of the FM-MBC before and after adsorption Cr(VI) were 24.33, 28.10, 7.62, 38.01 and 13.89, 4.21, 6.42, 49.32, respectively, and the means of mass percentages (%) of Cr of the FM-MBC after adsorption Cr(VI) was 22.32%. This pattern confirmed that hexavalent chromium was adsorbed on FM-MBC surface.

Table 3. Surface composition of the FM-MBC and FM-MBC after Cr(VI) adsorption by EDS analysis.

Element	C	O	Mn	Fe	Cr	Other
FM-MBC (wt. %)	24.33	28.10	7.62	38.01	-	1.94
FM-MBC after Cr(VI) adsorption (wt. %)	13.89	4.21	6.42	49.32	22.32	3.84

3.6.2. FTIR Analysis

The FTIR spectra of MBC, FM-MBC and FM-MBC after chromium adsorption were shown in Figure 8. Absorption band at the wave number (ν) values 3419 cm^{-1} was present in three spectra, which indicated the stretch and bending vibration modes of -OH [43]. The band at $\nu = 2894\text{ cm}^{-1}$ corresponded to the -CH₂ deformation vibration [44], and the band at $\nu = 1622\text{ cm}^{-1}$ corresponded to the vibration of aromatic groups (e.g., C = C) and carboxyl (C = O) [45]. Compared to MBC, some new bands at $\nu = 1428$, 1162, 1049, 876, 697, and 566 cm^{-1} were observed in FTIR spectra of FM-MBC. The bands at $\nu = 1428$, 1162, and 1049 cm^{-1} corresponded to the bending vibration of the Fe-OH and Mn-OH [40,46]. Meanwhile, the band at $\nu = 876\text{ cm}^{-1}$ could be due to Fe-OH vibrations of α -FeOOH. Besides, absorption band at the wave number (ν) values 697 and 566 cm^{-1} could be ascribed to α -Fe₂O₃ [40]. However, the bands at $\nu = 450$, 520, and 720 cm^{-1} due to the stretching vibrations of Mn-O were not found in the FTIR spectra of the FM-MBC. It could be the amorphization of MnO₂ in the FM-MBC, which corresponded to XRD characterization of FM-MBC [25]. The adsorption bands at $\nu = 1622$ and 1162 cm^{-1} became weakened in the FM-MBC after Cr(VI) adsorption than FM-MBC, and it could be seen that the band at $\nu = 1051\text{ cm}^{-1}$ of the FM-MBC shift from 1049 cm^{-1} to $\nu = 1051\text{ cm}^{-1}$ after Cr(VI) adsorption, which indicated that aromatic groups, carboxyls, and the hydroxyl groups associated with Fe and Mn involved in the adsorption process [40,46,47].

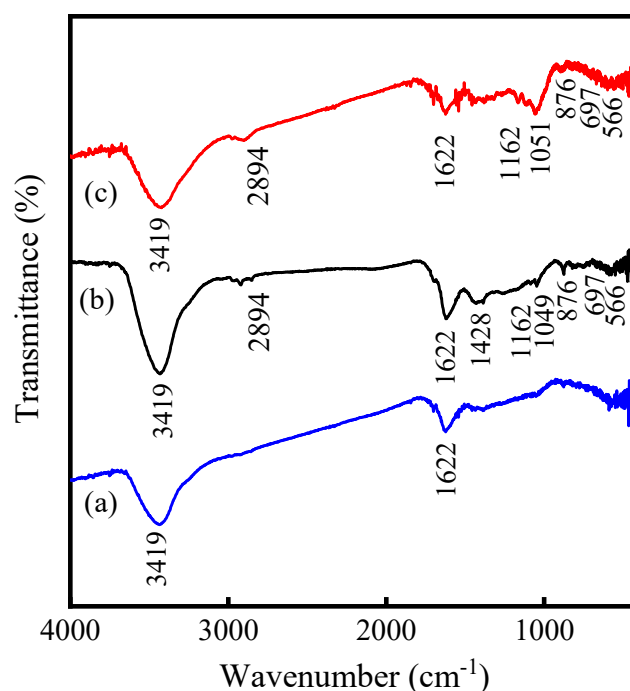


Figure 8. FTIR spectrum of MBC and FM-MBC. (a) MBC, (b) FM-MBC, (c) FM-MBC after Cr(VI) adsorption.

3.6.3. XPS Analysis

XPS spectrum of MBC and FM-MBC before and after adsorption Cr(VI) were shown in Figure 9. The photoelectron signals of MBC were C1s (284.05 eV) and O1s (531.52 eV). The photoelectron signals of FM-MBC and FM-MBC after Cr(VI) adsorption were C1s (284.40 eV), O1s (530.80 eV), Mn2p (640.90 eV), and Fe2p (710.50 eV). Because the strength of XPS is related to the content of elements, the content of Mn in FM-MBC before and after adsorption in Table 3 is only 6.42–7.62 wt. %, so the peak of Mn in XPS is not obvious. The peak center at 576.7 eV (spectrum FM-MBC after Cr(VI) adsorption) is due to the Cr2p, indicating that Cr(VI) was absorbed onto FM-MBC. This result was consistent with the results of FT-IR spectra of FM-MBC and the results of Yu et al. [48].

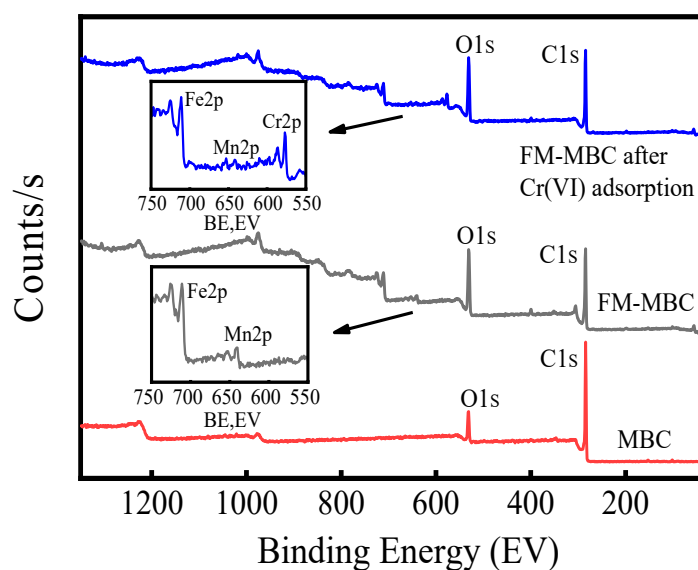


Figure 9. XPS of a full scan spectrum of MBC, FM-MBC and FM-MBC after Cr(VI) adsorption.

High-resolution XPS scans of the Fe2p orbital and Mn2p orbital on the FM-MBC surface before and after adsorption in the range of 700–740 eV and 635–660 eV were undertaken, respectively (Figure 10 and Table S3). The main Fe2p peak was shifted from 710.55 to 710.76 eV after Cr(VI) adsorption, which suggested iron oxide was involved in Cr(VI) adsorption onto FM-MBC. The binding energy of Mn2p was decreased from 640.48 to 641.03 eV after Cr(VI) adsorption. These values were typical of the valence state of Mn⁴⁺, which existed in the form of MnO₂ [49]. These results indicated that both Fe2p and Mn2p were involved in the adsorption reaction.

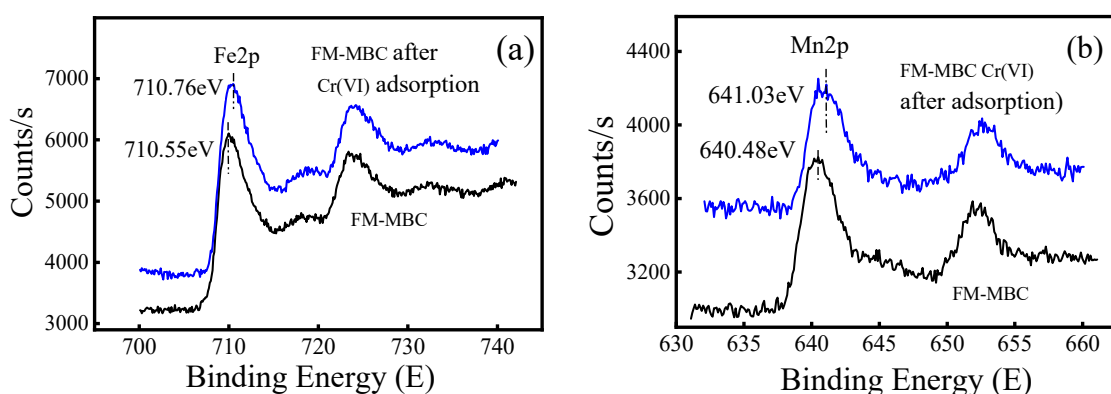
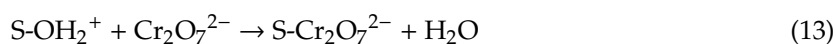


Figure 10. XPS spectra of FM-MBC before and after Cr(VI) adsorption, (a) Fe2p, (b) Mn2p.

On the surface of FM-MBC, there are a large number of functional groups on the surface of C-OH, Fe-OH, and Mn-OH (represented by S-OH); and -COOH (represented by S-COOH), when the pH = 2.0 < p*H*_{zpc}, the surface of FM-MBC was positively charged. The combination reaction between FM-MBC and Cr (VI) ions in solution with different forms may be assumed as follows (Equations (11)–(17)).



Moreover, it was supposed that Cr(VI) could adsorb onto the FM-MBC including electrostatic interaction, surface adsorption of Cr(VI) on FM-MBC, and the ion exchange between the surface functional groups of the FM-MBC with Cr(VI). The possible adsorption mechanism is illustrated in Figure 11.

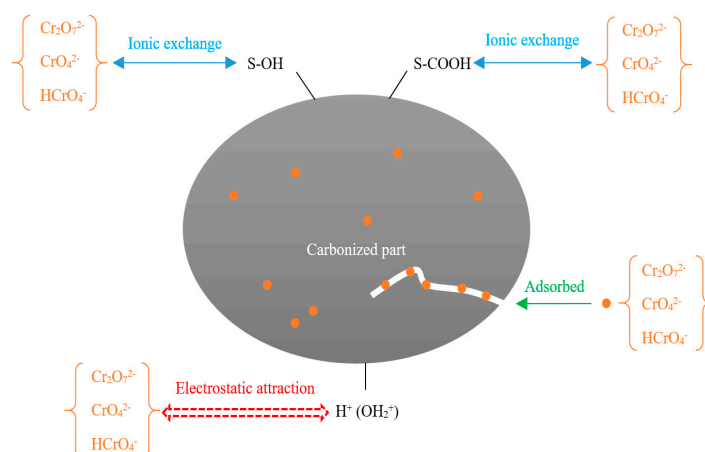


Figure 11. The proposed reaction mechanism of Cr(VI) on the FM-MBC.

4. Conclusions

There is nowadays a growing incentive for fit-for-purpose treatment methods to be developed for metal-containing wastewaters using low-cost materials. This study highlighted that Mulberry stem, an abundant biomass, can serve as a potential cheap source for the preparation of sorbents for hexavalent chromium removal. Loaded with α -Fe₂O₃ and amorphization of MnO₂ particles, FM-MBC had a microporous structure with a BET surface area of 74.73 m²/g, and the point of zero charge values (pH_{ZPC}) of FM-MBC was 7.4. Major carboxylic acid, hydroxyl, and carbonyls were present on the surface of FM-MBC. The optimum Cr(VI) adsorption occurred at pH 2.0. The pH of the optimal adsorption was acidity, which was the only disadvantage of the FM-MBC. At 25, 35, and 45 °C, the correlation coefficients of the Langmuir isotherm adsorption model were 0.999, 0.998, and 0.999, respectively, and the maximum adsorption capacities of Cr(VI) were 28.31, 31.02, and 37.14 mg/g, respectively. These results indicated that monolayer adsorption by the FM-MBC occurred. The process of FM-MBC adsorption Cr(VI) was a spontaneous and endothermic physical-chemical adsorption. The aromatic groups, carboxyls, and the hydroxyl groups associated with Fe and Mn were included in the adsorption process. The main mechanism of the Cr(VI) adsorption on FM-MBC mainly involved electrostatic interaction, surface adsorption of Cr(VI) on FM-MBC, and ion exchange.

Supplementary Materials: The following are available online at <http://www.mdpi.com/1660-4601/17/3/676/s1>, Figure S1: Zeta potential of FM-MBC as function of pH, Table S1: Composition analysis of MBC and FM-MBC before and after Cr(VI) adsorption, Table S2: Mineral element analysis of MBC and FM-MBC, Table S3: XPS peak spectral analysis of FM-MBC and FM-MBC after Cr(VI) adsorption.

Author Contributions: M.L. and Y.Z. conceived the concept and wrote the paper; S.X. did the experiment and wrote the paper, X.C., Z.D., and L.Y. read and commented on the manuscript; H.H. and Y.Z. revised the paper. All authors have read and agreed to the published version of the manuscript.

Funding: This work was supported by Guangxi Natural Science Foundation Project (No.:2017GXNSFAA198186), the National Natural Science Foundation of China under Grant (Grant No.: 21707024, 21367010, 51638006), and Guangxi science and Technology Planning Project under Grant (No.: GuiKe-AD18126018).

Acknowledgments: The authors would like to express their gratitude to EditSprings (<https://www.editsprings.com/>) for the expert linguistic services provided.

Conflicts of Interest: The authors declare no competing interests.

References

- Li, K.; Huang, Z.; Zhu, S.; Luo, S.; Yan, L.; Dai, Y.; Guo, Y.; Yang, Y. Removal of Cr(VI) from water by a biochar-coupled g-C₃N₄ nanosheets composite and performance of a recycled photocatalyst in single and combined pollution systems. *Appl. Catal. B Environ.* **2019**, *243*, 386–396. [CrossRef]

2. Kretschmer, I.; Senn, A.M.; Meichtry, J.M.; Custo, G.; Halac, E.B.; Dillert, R.; Bahnemann, D.W.; Litter, M.I. Photocatalytic reduction of Cr(VI) on hematite nanoparticles in the presence of oxalate and citrate. *Appl. Catal. B Environ.* **2019**, *242*, 218–226. [[CrossRef](#)]
3. Xu, X.Y.; Huang, H.; Zhang, Y.; Xu, Z.B.; Cao, X.D. Biochar as both electron donor and electron shuttle for the reduction transformation of Cr(VI) during its sorption. *Environ. Pollut.* **2019**, *244*, 423–430. [[CrossRef](#)] [[PubMed](#)]
4. Anandaraj, B.; Eswaramoorthi, S.; Rajesh, T.P.; Aravind, J.; Babu, S.P. Chromium(VI) adsorption by codium tomentosum: Evidence for adsorption by porous media from sigmoidal dose-response curve. *Int. J. Environ. Sci. Technol.* **2018**, *15*, 2595–2606. [[CrossRef](#)]
5. Andrade, J.K.; Andrade, C.K.; Felsner, M.L.; Anjos, V.E. Ultrasound-assisted emulsification microextraction combined with graphite furnace atomic absorption spectrometry for the chromium speciation in water samples. *Talanta* **2019**, *191*, 94–102. [[CrossRef](#)] [[PubMed](#)]
6. Zhou, L.; Liu, Y.G.; Liu, S.B.; Yin, Y.C.; Zeng, G.M.; Tan, X.F.; Hu, X.; Hu, X.J.; Jiang, L.H.; Ding, Y.; et al. Investigation of the adsorption-reduction mechanisms of hexavalent chromium by ramie biochars of different pyrolytic temperatures. *Bioresour. Technol.* **2016**, *218*, 351–359. [[CrossRef](#)]
7. An, Q.; Li, X.Q.; Nan, H.Y.; Yu, Y.; Jiang, J.N. The potential adsorption mechanism of the biochars with different modification processes to Cr(VI). *Environ. Sci. Pollut. Res.* **2018**, *25*, 31346–31357. [[CrossRef](#)]
8. Tian, X.K.; Wang, W.W.; Tian, N.T.; Zhou, C.X.; Yang, C.; Komarneni, S. Cr(VI) reduction and immobilization by novel carbonaceous modified magnetic Fe₃O₄/halloysite nanohybrid. *J. Hazard. Mater.* **2016**, *309*, 151–156. [[CrossRef](#)]
9. Hu, J.; Chen, G.H.; Lo, I.M. Removal and recovery of Cr(VI) from wastewater by maghemite nanoparticles. *Water Res.* **2005**, *39*, 4528–4536. [[CrossRef](#)]
10. Wang, M.C.; Sheng, G.D.; Qiu, Y.P. A novel manganese-oxide/biochar composite for efficient removal of lead(II) from aqueous solutions. *Int. J. Environ. Sci. Technol.* **2015**, *12*, 1719–1726. [[CrossRef](#)]
11. Yang, Y.Q.; Chen, N.; Feng, C.Q.; Li, M.; Gao, Y. Chromium removal using a magnetic corncob biochar/polypyrrole composite by adsorption combined with reduction: Reaction pathway and contribution degree. *Colloids Surf.* **2018**, *556*, 201–209. [[CrossRef](#)]
12. Myung, Y.; Jung, S.; Tung, T.T.; Tripathi, K.M.; Kim, T.Y. Graphene-Based Aerogels Derived from Biomass for Energy Storage and Environmental Remediation. *ASC. Sustain. Chem. Eng.* **2019**, *7*, 3772–3782. [[CrossRef](#)]
13. Liu, N.; Zhang, Y.T.; Xu, C.; Liu, P.; Lv, J.; Liu, Y.Y.; Wang, Q.Y. Removal mechanisms of aqueous Cr(VI) using apple wood biochar: Aspectroscopic study. *J. Hazard. Mater.* **2020**, *384*, 121371. [[CrossRef](#)] [[PubMed](#)]
14. Liao, F.; Yang, L.; Li, Q.; Li, Y.R.; Yang, L.T.; Anas, M.; Huang, D.L. Characteristics and inorganic N holding ability of biochar derived from the pyrolysis of agricultural and forestal residues in the southern China. *J. Anal. Appl. Pyrol.* **2018**, *134*, 544–551. [[CrossRef](#)]
15. Correa, F.G.; Bulbulian, S. Co(II) adsorption in aqueous media by a synthetic Fe-Mn binary oxide adsorbent. *Water Air Soil Pollut.* **2012**, *223*, 4089–4100. [[CrossRef](#)]
16. Taffarel, S.R.; Rubio, J. Removal of Mn²⁺ from aqueous solution by manganese oxide coated zeolites. *Miner. Eng.* **2010**, *23*, 1131–1138. [[CrossRef](#)]
17. Aryal, M.; Ziaigova, M.; Kyriakides, M.L. Comparison of Cr(VI) and As(V) removal in single and binary mixtures with Fe(III)-treated Staphylococcus xylosus biomass: Thermodynamic studies. *Chem. Eng. J.* **2011**, *169*, 100–106. [[CrossRef](#)]
18. Cui, H.J.; Cai, J.K.; Zhao, H.; Yuan, B.L.; Ai, C.L.; Fu, M.L. Fabrication of magnetic porous Fe-Mn binary oxide nanowires with superior capability for removal of As(III) from water. *J. Hazard. Mater.* **2014**, *279*, 26–31. [[CrossRef](#)]
19. Wang, W.L.; Fu, X.B. Efficient Removal of Cr(VI) with Fe/Mn Mixed Metal Oxide Nanocomposites Synthesized by a Grinding Method. *J. Nanomater.* **2013**, *2013*, 7.
20. Wen, Z.P.; Zhang, Y.L.; Guo, S.; Chen, R. Facile template-free fabrication of iron manganese bimetal oxides nanospheres with excellent capability for heavy metals removal. *J. Colloid Interface Sci.* **2017**, *486*, 211–218. [[CrossRef](#)]
21. Du, X.L.; Yu, Z.Y.; Zhu, Y.J. Cr(VI) adsorption from aqueous solution and its reactions behavior on the surfaces of granular Fe-Mn binary oxides. *Environ. Prog. Sustain.* **2019**, *38*, S176–S184. [[CrossRef](#)]

22. Lu, J.B.; Liu, H.J.; Zhao, X.; Jefferson, W.; Cheng, F.; Qu, J.H. Phosphate removal from water using freshly formed Fe-Mn binary oxide: Adsorption behaviors and mechanisms. *Colloids Surf. A Physicochem. Eng. Asp.* **2014**, *455*, 11–18. [[CrossRef](#)]
23. Wu, Z.B.; Zhong, H.; Yuan, X.Z.; Wang, H.; Wang, L.L.; Chen, X.H.; Zeng, G.M.; Wu, Y. Adsorptive removal of methylene blue by rhamnolipid-functionalized graphene oxide from wastewater. *Water Res.* **2014**, *67*, 330–344. [[CrossRef](#)] [[PubMed](#)]
24. Beesley, L.; Marmiroli, M. The immobilisation and retention of soluble arsenic, cadmium and zinc by biochar. *Environ. Pollut.* **2011**, *159*, 474–480. [[CrossRef](#)] [[PubMed](#)]
25. Xiong, Y.; Tong, Q.; Shan, W.J.; Xing, Z.Q.; Wang, Y.J.; Wen, S.Q. Arsenic transformation and adsorption by iron hydroxide/manganese dioxide doped straw activated carbon. *Appl. Surf. Sci.* **2017**, *416*, 618–627. [[CrossRef](#)]
26. Joshi, T.P.; Zhang, G.; Koju, R.; Qi, Z.L.; Liu, R.P.; Liu, H.J.; Qu, J.H. The removal efficiency and insight into the mechanism of para arsanilic acid adsorption on Fe-Mn framework. *Sci. Total Environ.* **2017**, *601*, 713–722. [[CrossRef](#)]
27. Zhu, Y.E.; Li, H.; Zhang, G.X.; Meng, F.J.; Li, L.F.; Wu, S. Removal of hexavalent chromium from aqueous solution by different surface-modified biochars: Acid washing, nanoscale zero-valent iron and ferric iron loading. *Bioresour. Technol.* **2018**, *261*, 142–150. [[CrossRef](#)]
28. Lian, F.; Xing, B.S. Black carbon (biochar) in water/soil environments: Molecular structure, sorption, stability, and potential risk. *Environ. Sci. Technol.* **2017**, *51*, 13517–13532. [[CrossRef](#)]
29. Mohan, D.; Pittman Jr, C.U. Activated carbons and low cost adsorbents for remediation of tri- and hexavalent chromium from water. *J. Hazard. Mater.* **2006**, *137*, 762–811. [[CrossRef](#)]
30. Zhang, W.; Zhang, S.; Wang, J.; Wang, M.; He, Q.L.; Song, J.Y.; Wang, H.Y.; Zhou, J.P. Hybrid functionalized chitosan-Al₂O₃@SiO₂ composite for enhanced Cr(VI) adsorption. *Chemosphere* **2018**, *203*, 188–198. [[CrossRef](#)]
31. Brandão, P.C.; Souza, T.C.; Ferreira, C.A.; Hori, C.E.; Romanielo, L.L. Removal of petroleum hydrocarbons from aqueous solution using sugarcane bagasse as adsorbent. *J. Hazard. Mater.* **2010**, *175*, 1106–1112. [[CrossRef](#)] [[PubMed](#)]
32. Liang, M.N.; Wang, D.Q.; Zhu, Y.N.; Zhu, Z.Q.; Li, Y.H.; Huang, C.P. Nano-hematite bagasse composite (n-HBC) for the removal of Pb(II) from dilute aqueous solutions. *J. Water Process Eng.* **2018**, *21*, 69–76. [[CrossRef](#)]
33. Wang, F.; Liu, L.Y.; Liu, F.; Wang, L.G.; Ouyang, T.; Chang, C.T. Facile one-step synthesis of magnetically modified biochar with enhanced removal capacity for hexavalent chromium from aqueous solution. *J. Taiwan Inst. Chem. Eng.* **2017**, *81*, 414–418. [[CrossRef](#)]
34. Hu, Z.L.; Cai, L.M.; Liang, J.M.; Guo, X.T.; Li, W.; Huang, Z.J. Green synthesis of expanded graphite/layered double hydroxides nanocomposites and their application in adsorption removal of Cr(VI) from aqueous solution. *J. Clean. Prod.* **2019**, *209*, 1216–1227. [[CrossRef](#)]
35. Sheikhmohammadi, A.; Hashemzadeh, B.; Alinejad, A.; Mohseni, S.M.; Sardar, M.; Sharafkhani, R.; Sarkhosh, M.; Asgari, E.; Bay, A. Application of graphene oxide modified with the phenopyridine and 2-mercaptobenzothiazole for the adsorption of Cr(VI) from wastewater: Optimization, kinetic, thermodynamic and equilibrium studies. *J. Mol. Liq.* **2019**, *285*, 586–597. [[CrossRef](#)]
36. Rossi, A.D.; Rigon, M.R.; Zapparoli, M.; Braido, R.D.; Colla, L.M.; Dotto, G.L.; Piccin, J.F. Chromium (VI) biosorption by *Saccharomyces cerevisiae* subjected to chemical and thermal treatments. *Environ. Sci. Pollut. Res.* **2018**, *25*, 19179–19186. [[CrossRef](#)]
37. Chen, T.; Zhou, Z.Y.; Xu, S.; Wang, H.T.; Lu, W.J. Adsorption behavior comparison of trivalent and hexavalent chromium on biochar derived from municipal sludge. *Bioresour. Technol.* **2015**, *190*, 388–394. [[CrossRef](#)]
38. Choudhary, B.; Paul, D. Isotherms, kinetics and thermodynamics of hexavalent chromium removal using biochar. *J. Environ. Chem. Eng.* **2018**, *6*, 2335–2343. [[CrossRef](#)]
39. Gode, F.; Pehlivan, E. Removal of Cr(VI) from aqueous solution by two Lewatit anion exchange resins. *J. Hazard. Mater.* **2005**, *119*, 175–182. [[CrossRef](#)]
40. Song, Z.G.; Lian, F.; Yu, Z.H.; Zhu, L.Y.; Xing, B.S.; Qiu, W.W. Synthesis and characterization of a novel MnOx-loaded biochar and its adsorption properties for Cu²⁺ in aqueous solution. *Chem. Eng. J.* **2014**, *242*, 36–42. [[CrossRef](#)]

41. Zhu, Z.Q.; Zhu, Y.N.; Yang, F.; Zhang, X.H.; Qin, H.; Liang, Y.P.; Liu, J. Sorption-reduction removal of Cr(VI) from aqueous solution by the porous biomorph-genetic composite of α -Fe₂O₃/Fe₃O₄/C with eucalyptus wood hierarchical microstructure. *Desalin. Water Treat.* **2014**, *52*, 3133–3146. [[CrossRef](#)]
42. Crini, G. Kinetic and equilibrium studies on the removal of cationic dyes from aqueous solution by adsorption onto a cyclodextrin polymer. *Dye. Pigment* **2008**, *77*, 415–426. [[CrossRef](#)]
43. Gupta, V.K.; Nayak, A.; Agarwal, S.; Dobhal, R.; Uniyal, D.P.; Singh, P. Arsenic speciation analysis and remediation techniques in drinking water. *Desalin. Water Treat.* **2012**, *40*, 231–243. [[CrossRef](#)]
44. Chen, B.L.; Chen, Z.M.; Lv, S.F. A novel magnetic biochar efficiently sorbs organic pollutants and phosphate. *Bioresour. Technol.* **2011**, *102*, 716–723. [[CrossRef](#)] [[PubMed](#)]
45. Du, L.; An, S.W.; Ding, J.; Jiang, D.; Hong, W.; Jin, Y.D.; Liu, L.; Wang, R.B.; Zhang, D.; Xia, C.Q. Adsorption and desorption of uranium(VI) by Fe-Mn binary oxide in aqueous solutions. *J. Radioanal. Nucl. Chem.* **2016**, *308*, 545–554. [[CrossRef](#)]
46. Xu, W.; Wang, H.J.; Liu, R.P.; Zhao, X.; Qu, J.H. The mechanism of antimony(III) removal and its reactions on the surfaces of Fe-Mn Binary Oxide. *J. Colloid Interface Sci.* **2011**, *363*, 320–326. [[CrossRef](#)]
47. Wang, X.S.; Chen, L.F.; Li, F.Y.; Chen, K.L.; Wan, W.Y.; Tang, Y.J. Removal of Cr(VI) with wheat-residue derived black carbon: Reaction mechanism and adsorption performance. *J. Hazard. Mater.* **2010**, *175*, 816–822. [[CrossRef](#)]
48. Yu, Z.H.; Zhang, X.D.; Huang, Y.M. Magnetic chitosan-iron(III) hydrogel as a fast and reusable adsorbent for chromium(VI) removal. *Ind. Eng. Chem. Res.* **2013**, *52*, 11956–11966. [[CrossRef](#)]
49. Maliyekkal, S.M.; Lisha, K.P.; Pradeep, T. A novel cellulose-manganese oxide hybrid material by in situ soft chemical synthesis and its application for the removal of Pb(II) from water. *J. Hazard. Mater.* **2010**, *181*, 986–995. [[CrossRef](#)]



© 2020 by the authors. Licensee MDPI, Basel, Switzerland. This article is an open access article distributed under the terms and conditions of the Creative Commons Attribution (CC BY) license (<http://creativecommons.org/licenses/by/4.0/>).